Available online at www.sciencedirect.com

SCIENCE DIRECT®

Developmental Biology 270 (2004) 31–46

DEVELOPMENTAL BIOLOGY

www.elsevier.com/locate/ydbio

A *Titin* mutation defines roles for circulation in endothelial morphogenesis

Scott R. May, Nicola J. Stewart, Wesley Chang, and Andrew S. Peterson*

Department of Neurology and the Gallo Center, University of California at San Francisco, Emeryville, CA 94608, USA

Received for publication 5 September 2003, revised 26 December 2003, accepted 10 February 2004

Available online 14 March 2004

Abstract

Morphogenesis of the developing vascular network requires coordinated regulation of an extensive array of endothelial cell behaviors. Precisely regulated signaling molecules such as vascular endothelial growth factor (VEGF) direct some of these endothelial behaviors. Newly forming blood vessels also become subjected to novel biomechanical forces upon initiation of cardiac contractions. We report here the identification of a recessive mouse mutation termed shrunken-head (shru) that disrupts function of the *Titin* gene. *Titin* was found to be required for the initiation of proper heart contractions as well as for maintaining the correct overall shape and orientation of individual cardiomyocytes. Cardiac dysfunction in shrunken-head mutant embryos provided an opportunity to study the effects of lack of blood circulation on the morphogenesis of endothelial cells. Without blood flow, differentiating endothelial cells display defects in their shapes and patterns of cell–cell contact. These endothelial cells, without exposure to blood circulation, have an abnormal distribution within vasculogenic vessels. Further effects of absent blood flow include abnormal spatial regulation of angiogenesis and elevated VEGF signaling. The shrunken-head mutation has provided an in vivo model to precisely define the roles of circulation on cellular and network aspects of vascular morphogenesis.

Keywords: Vascular development; Mouse; Heart; Genetics; Mutagenesis; ENU

Introduction

The vasculature begins to form during gastrulation, initially in extraembryonic tissues that form the yolk sac and subsequently in the embryo itself. Shortly after gastrulation, the heart begins to form when two bilateral fields of cardiac precursors converge toward the midline. After fusion of these two fields, future cardiomyocytes arrange in a single cell layer surrounding the underlying layer of endocardium. This linear heart tube begins to spontaneously contract by 8.5 days post coitus (DPC) in the mouse, thereby exposing developing endothelial cells to new biomechanical stimuli. Subsequent growth and morphogenesis of the heart yields a rhythmically contracting organ that circulates blood throughout the embryo. After the onset of circulation, the primitive vascular pattern is further expanded and refined by angiogenesis, the formation of vessels through sprouting and remodeling from existing vessels.

Morphogenesis of the vasculature utilizes a variety of mechanisms that regulate cell behavior. Angioblasts use environmental cues to migrate various distances depending on the vessel to which they will contribute (Coffin and Poole, 1991; Drake et al., 1998; Sugi and Markwald, 1996). Following migration, angioblasts engage a protrusive activity of their plasma membranes whereby these cellular extensions recognize neighboring angioblasts and form cellular adhesions. While these cord-like cellular assemblies are forming, primordial ECs thin, flatten, and assume the spindle shape characteristic of differentiated ECs. Precise regulations of protrusive activity and cellular and extracellular matrix (ECM) contacts are believed to align primordial ECs at the vertices of vascular polygons. Tensional forces can then create a single cell-layered vascular lumen. Continued vascular fusion can combine neighboring small caliber vessels into larger ones (Drake and Little, 1999).

These morphogenetic events are beginning to be understood at the molecular level. Growth factor signaling and communication between ECs and with the ECM are all integrated during these cellular behaviors. Vascular endothelial growth factor (VEGF) stands as a particularly important regulator of vascular morphogenesis. Several VEGF

* Corresponding author. Department of Neurology and the Gallo Center, University of California at San Francisco, 5858 Horton Street, Emeryville, CA 94608. Fax: +1-510-985-3101.

E-mail address: andpete@itsa.ucsf.edu (A.S. Peterson).

0012-1606/$ - see front matter © 2004 Elsevier Inc. All rights reserved.
doi:10.1016/j.ydbio.2004.02.006

isoforms, differing in their diffusion properties, are secreted from a variety of cell types surrounding areas of active vessel formation (Miquerol et al., 1999). VEGF signaling involves two endothelial specific receptor tyrosine kinases, Flt-1 (also known as VEGFR-1) and Flk-1 (also known as VEGFR-2), as well as two co-receptors, neuropilin-1 and -2 ((de Vries et al., 1992; Terman et al., 1992 #28; Soker et al., 1998 #25; Gluzman-Poltorak et al., 2000)). VEGF has been demonstrated to serve as a chemoattractant during angioblast migration (Cleaver and Krieg, 1998). Components of the ECM, such as fibronectin, are also believed to provide both supportive and instructive roles during this migration process (Risau and Lemmon, 1988). In addition to its described roles in EC migration and proliferation (Plouet et al., 1989), VEGF mediates EC protrusive activity (Drake et al., 2000) as well as vascular fusion (Drake and Little, 1995). To accommodate its variety of functions, precise regulation of VEGF bioavailability is critical for proper vascular development (Carmeliet et al., 1996). This regulation occurs transcriptionally, posttranscriptionally, and through VEGF's interactions with proteins that both inhibit (Flt-1 and SPARC) or help to activate (Flk-1 and Neuropilin-1 and -2) VEGF signaling (Ferrara, 1999). Additional investigation into the pathological alterations of VEGF activity will undoubtedly yield new insights into how this signaling pathway can alter vascular function in vivo.

Vasculogenesis creates lumenized vessels before circulation. With the onset of heart contractions, these vessels are subjected to new biomechanical and biochemical stimuli that result from circulation. It has been clearly demonstrated both in vitro and in vivo that the functional phenotype of vascular endothelium is dynamically responsive to an array of biomechanical stimuli that result from circulation. Cultured endothelial cells exposed to fluid shear stresses undergo a variety of cell shape alterations. Changes in the distribution of actin-containing stress fibers result in cultured ECs aligning with the direction of flow and elongating their cell bodies (Dewey et al., 1981; Frame and Sarelius, 2000). Shear stresses can also alter the position of the microtubule organizing complex, the Golgi apparatus, and the nucleus of ECs (Coan et al., 1993). The number and distribution of focal adhesions change in response to shear stress, and cultured ECs tend to migrate away from the source of flow (Li et al., 2002). It is noteworthy that many of these in vitro responses to shear stress mimic aspects of vessel morphogenesis that occur in vivo. Blood flow has been shown to direct angiogenic growth and remodeling within the extraembryonic yolk sac (Koushik et al., 2001; Luo et al., 2001) as well as regulate glomerular morphogenesis within the kidney (Serluca et al., 2002). However, it is not clear what distinct steps of vessel morphogenesis are affected by lack of circulation within the embryo because vessel development has not been thoroughly studied in mouse models immediately following primary cardiac defects.

In this paper, we describe the localization and phenotypic characterization of a mutation in the mouse *Titin* gene. Titin proteins are megadalton-sized filamentous molecules that function as molecular springs in striated muscle (reviewed in (Tskhovrebova and Trinick, 2002). Titin function is of critical importance for muscle elasticity as well as structural integrity of the sarcomere. Various mutations in *Titin* have been shown to cause heart failure in the form of dilated cardiomyopathy (Gerull et al., 2002; Xu et al., 2002) or skeletal muscular dystrophy (Garvey et al., 2002; Hackman et al., 2002). The shrunken-head (shru) mutation allowed us to study *Titin*'s role in the development of the mouse heart. Hearts of mutant embryos displayed weak spontaneous contractions from the outset and never developed a strong, regular contractile rhythm. The initiation of blood circulation occurred over a day later in mutants than in wild-type embryos. Shru hearts did not become dilated as occurs with other characterized Titin mutations such as *pickwick*^{m171} (*pik*^{m171}) (Xu et al., 2002). Instead, both the myocardial and endocardial cells in shru hearts were misaligned. Because the shru mutant phenotype produces weak heart contractility, this also provided an opportunity for a thorough study of the immediate and protracted effects that lack of circulation has on blood vessel morphogenesis. Vessel lumen maintenance was disrupted and ECs were mispositioned along the anterior–posterior (A–P) axis as part of the novel vascular defects seen in shru embryos shortly after the delay of circulation. Defects in endothelial shape and cell–cell contacts are believed to be mechanistic causes for these specific vessel assembly errors. Vessels then quickly developed large dilations and underwent aberrant sprouting and pruning indicating that angiogenesis was misregulated. Elevated VEGF expression and a genetic interaction between shru and *Flt-1* indicated that absent circulation produced abnormal VEGF signaling which likely contributed to the vascular defects in mutant embryos. In the process of characterizing shru, a new role for *Flt-1* in controlling EC number was also identified. Analysis of the *shrunken-head* mutation has defined the in vivo roles of cardiac function in directing specific endothelial cell behaviors that elicit vascular morphogenesis.

Materials and methods

Mapping

A set of 96 PCR-based simple sequence length polymorphism (SSLP) markers from the Whitehead Institute Center for Genome Research (Dietrich et al., 1995) spaced at 20-cm intervals throughout the genome was used for linkage analysis. Polymorphisms were distinguished via polyacrylamide gel electrophoresis using an ABI 377 (Perkin-Elmer, Boston, MA). Additional chromosome 2 SSLP markers derived at the Whitehead Institute (www.genome.wi.mit.edu) were used for fine scale mapping. Testing regions of the shru interval using Celera's draft sequence also identified single nucleotide polymorphisms

and SSLPs. This marker information is available from the corresponding author. Two physical maps of the shru interval were constructed. One used a PCR-based assay on a mouse–hamster radiation hybrid mapping panel (Research Genetics, Huntsville, AL). A 5-fold coverage BAC contig was created by screening the library RPCI-23 (ResGen) and walking from marker D2Mit435 to D2Mit183. Both of these physical maps were used to confirm the accuracy of public and private draft DNA sequences of the shru interval.

Genotyping

Genotyping of *shru* carrier mice and mutant embryos was accomplished using PCR analysis of two SSLP markers that flank the *shrunken-head* locus. *D2Mit37* resides 1.1 cm proximal and *D2Mit159* lies 0.7 cm distal to the mutation. Polymorphisms between alleles on the mutant BTBR strain and wild-type C57Bl/6J or Cast/Ei strains were distinguished using 3.5% agarose gel electrophoresis.

Computational analysis of the shru genomic interval

Annotation of the shru genomic interval began with Celera's prediction of exons. BLAST analysis revealed that all predicted exons in the interval had previously been attributed to orthologous exons from human Titin transcripts (Bang et al., 2001). The shru genomic interval was also analyzed using the following gene prediction programs: GeneMarkTM (Georgia Institute of Technology), Perceval (Oak Ridge National Laboratory), and Genotator (University of Washington). None of the programs predicted coding sequences that were not previously ascribed as part of *Titin*. BLAST analysis of the 177-kb shru interval revealed no indication of any part of a gene other than *Titin*. The GenBank entry AL928789 contains sequence data for a BAC (RP23-435F21) from the contig that spans most of the interval. Analysis of these sequence data confirmed the continuity of Celera's draft sequence and was used to fill in three small sequence gaps in the shru interval.

Cell death assay

For whole-mount detection of cell death, 8.75 DPC embryos were first dissected, then rinsed in Pannett and Compton's saline (PCS), and incubated in Nile Blue A sulfate salt (0.2 mg/ml) in PCS for 20 min at 37°C. The embryos were then destained in PCS until the background clarified. Images were taken immediately using a Leica M420 microscope and NIH Image 1.62 software.

RT-PCR

Total RNA (1 μg) from 12 to 13 somites embryos was reverse transcribed using random hexamer primers (Invitrogen, Carlsbad, CA) and SuperScriptII RT (Invitrogen) at 25°C for 10 min and then 42°C for 50 min. PCR was carried out using these primer pairs:

β-actin: 5′ CTGTATGCCTCTGGTCGTAC, 5′ GGATGTCAACGTCACACTTC
Titin: 5′ TTCCAGAGTCATCACGGGTA, 5′ GAGTACCAGTTCCGTCTCAA
VEGF-A: 5′AGTGGTCCCAGGCTGCACC, 5′ GTCTTTCTTTGGTCTGCATTCA

The following number of PCR cycles were used for Fig. 7A (β-actin, 19 cycles. Titin, 24 cycles. VEGF-A, 27 cycles). Each PCR was also performed using both fewer and additional cycles to confirm that expression was being assayed within the pseudo-linear phase of amplification.

LacZ histochemistry and histological analysis

β-galactosidase activity was detected in *flt-shru* embryos following the protocol of Hogan et al. (1994). Embryos were dehydrated in an ethanol series, embedded in Paraplast Plus paraffin (Fisher), and sectioned at 10 μm. For histological analysis, 10-μm paraffin sections were stained with Lee's methylene blue-basic fuchsin dyes (Bennett et al., 1976).

Antibody staining and endothelial cell quantification

Immunofluorescence and whole-mount immunohistochemistry were performed using a primary antibody directed against the endothelial marker PECAM-1 (MEC13.3, rat anti-mouse monoclonal, Pharmingen). For fluorescence staining, 10-μm cryostat sections were incubated with MEC13.3 (1:60 dilution). AlexaFluor488-conjugated goat anti-rat secondary antibodies (1:500 dilution, Molecular Probes) were used to detect MEC13.3 localization. The DNA-binding dye Hoechst 2258 (0.4 mg/ml) was used to stain nuclei. Slides were then analyzed using a Leica DMRB microscope and Spot32 (Diagnostic Instruments, Inc.) imaging software. Whole-mount immunostaining of embryos with MEC13.3 (1:110 dilution) was performed as described (Suri et al., 1996) using the Vectastain ABC developing kit (Vector Laboratories).

For the EC quantification, every third 10-μm section from level of the cardiac inflow tract to the yolk sac vascular connection was collected. PECAM-1 and Hoechst staining identified individual ECs comprising the dorsal aortae.

Results

Identification of shrunken-head

The *shrunken-head* mutant was isolated in a genetic screen designed to identify recessive mutations that produce

novel developmental defects. Male BTBR mice were treated with ethyl-nitroso-urea (ENU) and bred to create a founding population of mice harboring random germ-line mutations. The resulting G0 males were backcrossed for two generations to C57Bl/6J females. Dissecting the litters from G2 females mated with their G1 father at 10.5 DPC allowed individual lines of mice to be assayed for recessive developmental phenotypes (Hentges et al., 1999). One of the mutations, shrunken-head, produces a phenotype that includes reduced growth of the head, a defective cardiovascular system, and regionally restricted increases in cell death.

Mapping of the shrunken-head gene

To facilitate identification of carrier animals and mutant embryos by genotyping and to allow candidates for the shru locus to be evaluated, the mutation was meiotically mapped. Initially, linkage to the middle of chromosome 2 was established using DNA from 12 known heterozygous shru carriers. Genotyping and testing of additional animals indicated that the mutation was fully penetrant on different genetic backgrounds. This allowed high-resolution mapping to proceed. To utilize a higher degree of polymorphism for the mapping process, shru was crossed from *Mus musculus domesticus* onto a more distantly related subspecies of mouse, *Mus musculus castaneus*. Over 10,000 meioses were scored using additional chromosome 2 markers, leading to a non-recombinant interval containing the shrunken-head locus that spans 177 kb of genomic sequence (Fig. 1A).

The shru mutation resides within the gene for Titin

The availability of draft sequence of the mouse genome from both the public sequencing effort and Celera greatly aided mapping of the shru locus. Genetic mapping information was rapidly correlated with a detailed physical map provided from Celera's draft sequence. The continuity and orientation of Celera's draft sequence covering the shru interval were confirmed through haplotype analysis of *shru* recombinants, by creating a BAC contig of the interval, and by analyzing marker loci using a mouse–hamster radiation hybrid mapping panel (data not shown). The mouse BAC RP23-435F21 contains DNA covering most of the shru interval and was sequenced by the Wellcome Trust Sanger Institute. Analysis of this sequence also confirmed the size and continuity of the shru interval.

The 177-kb non-recombinant interval was found to reside within the 3′ portion of the *Titin* gene (Fig. 1B). The *Titin* locus produces giant filamentous proteins expressed in cardiac and skeletal muscle. Titin filaments have been demonstrated to serve as structural components within muscle fibers, providing an extensible scaffold for the contractile machinery. Titins are required for elasticity as well as structural integrity of muscle fibers. Extensive computational analysis of this interval has yielded 272 predicted exons, all of which have been ascribed to at least one of *Titin*'s many transcripts. We therefore conclude that disruption of *Titin* function produces the *shru* phenotype. Levels of Titin mRNA expression remained unchanged in *shru* mutants (Fig. 7A). During mid-gestation of the mouse, *Titin* is expressed in the myocardium of the heart and in the somites (Schaart et al., 1989). *Titin*'s mRNA expression pattern was unchanged in mutants (data not shown). Loss of *Titin* function in *shru* results in cardiac failure followed by defective vascular morphogenesis and increased mesenchymal cell death.

Titin regulates cardiomyocyte shape and alignment

Mutations in *Titin* are known to cause dilated cardiomyopathy in humans and zebrafish (Gerull et al., 2002; Xu et al., 2002). *Shru* hearts are weakly contractile from the outset, develop pericardial edema by 9.5 DPC, and progressively fail. Mutant hearts appeared normal at 8.25 DPC (data not shown). Shortly after the first visual appearance of cardiac defects, mutant embryos were sectioned at 8.75 DPC and histologically stained to examine heart morphology (Fig. 2). Overall, *shru* hearts appeared neither dilated nor hypertrophic. Cells of both the myocardium and endocardium normally align smoothly to create a single cell layer of each tissue, separated by deposited ECM called cardiac jelly. Individual cardiomyocytes in *shru* hearts did not become distended as occurs with mutation in zebrafish *Titin*. In addition, the number and extent of trabecular projections from the myocardium into the cardiac jelly were reduced in the mutants, indicating defective endocardial and myocardial cellular interaction. Despite its poor contractility and lack of circulation, *shru* hearts underwent normal cardiac looping morphogenesis and proper regionalization as assayed by dHAND and eHAND expression (data not shown).

Developmental defects outside of the heart

Shrunken-head embryos exhibited a variety of developmental defects both within and outside of *Titin*'s expression domain (Fig. 3). *Shru* embryos could first be distinguished from their wild-type littermates at 8.5 days of gestation based on the exterior appearance of the heart. During the subsequent 24 hours of development, an overall reduction in growth, most prominent in the head, was seen. Immediately following the normal onset of cardiac contractions, 8.75 DPC *shru* embryos showed apparent necrosis in the frontonasal mesenchyme. By 9.0 DPC, the mandibular component of the first branchial arch, the region of head mesenchyme in apposition to the forebrain neurectoderm, and the interior of the somites (the scleratomal precursor region) became hollow, indicating a loss of particular cell types (Figs. 3E and F; and data not shown).

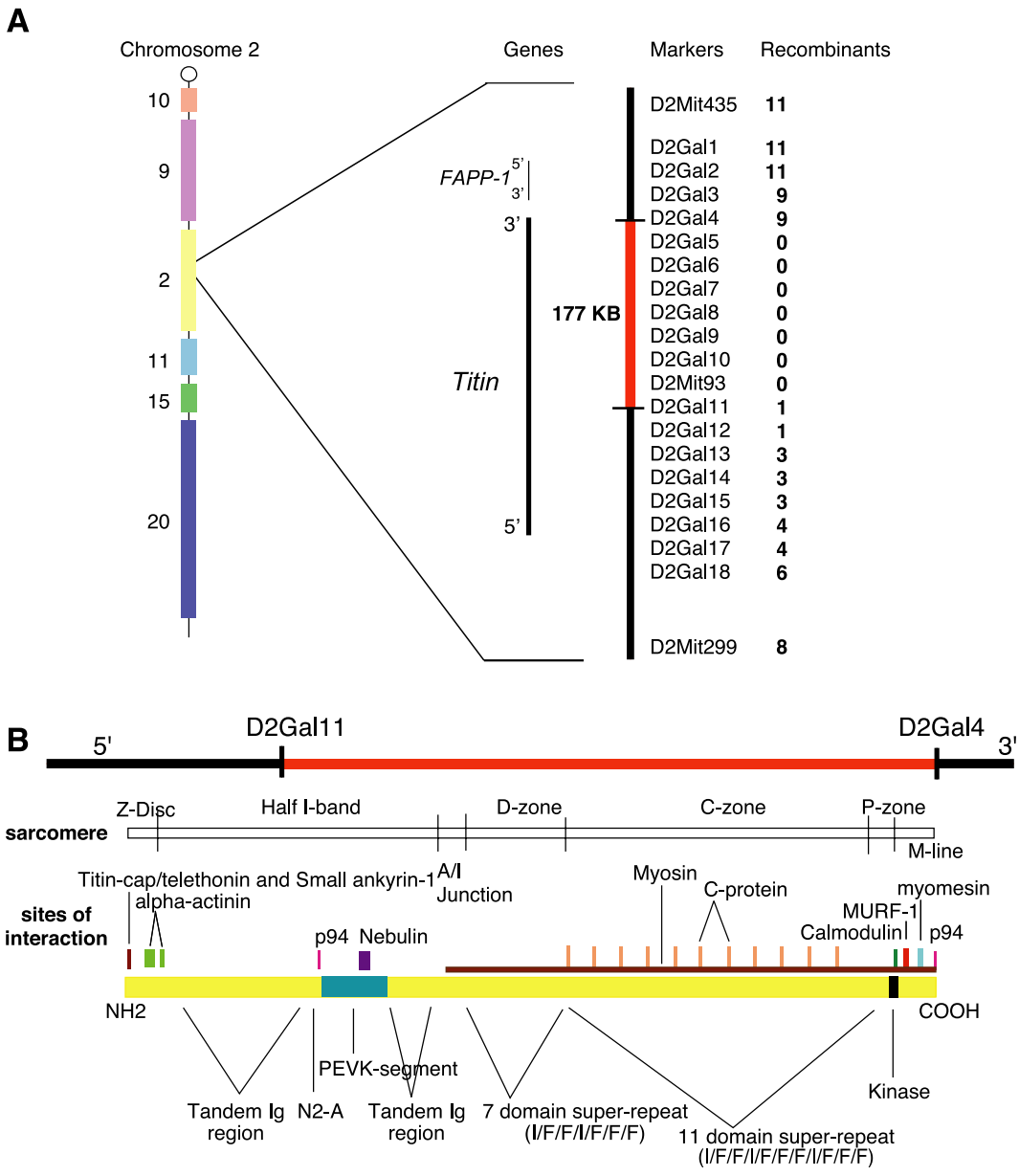

Fig. 1. Genetic mapping of the shrunken-head mutation within the Titin gene. (A) *Shru* was meiotically mapped to the long arm of chromosome 2 in a region that is homologous to human chromosome 2q31. Markers D2Gal4 and D2Gal11 define a non-recombinant genetic interval that is 177 kb. This interval resides within the gene for *Titin* (*Ttn*). (B) D2Gal4 lies in the 3′ UTR of Titin. D2Gal11 lies in between *Titin* exons 91 and 92. This section of the locus resides within the I-band region of Titin, encoding the carboxy portion of the proximal tandem Ig segment. This annotation depicts the layout of Titin filaments within the half-sarcomere, Titin's known protein interaction domains and Titin's own domain structure.

The specific pattern of cell loss in the head and somites of mutant embryos could result from cell death, inappropriate cell-type specification, decreases in proliferation, or aberrant cell migration. To investigate the idea that cell death was the cause, we used the vital dye Nile Blue Sulfate. Embryos (8.75 DPC) were stained and examined in whole-mount (Fig. 4). Wild-type embryos exhibited a scattered staining pattern with higher levels in structures such as the otic vesicles and rhombencephalic roof. Mutant embryos had staining in addition to that seen in wild-type embryos. The elevated staining pattern in mutants at 8.75 DPC was entirely consistent with the pattern of later cell loss. Increased staining levels were seen in the somites (Fig. 4D) and in the mesenchyme of the frontonasal mass and of the first branchial arch (Fig. 4B). Localized increases in cell death therefore account for the absence of these particular cell populations in *shrunken-head* mutants.

Defects in the function and architecture of the vascular system were readily apparent in shru embryos. Weakly contractile shru hearts failed to initiate embryonic circulation (Figs. 3A, D, and G). Once circulation did begin after 9.5 DPC, local areas of hemorrhage, prominent in the head, branchial arches, and limb buds, were present throughout

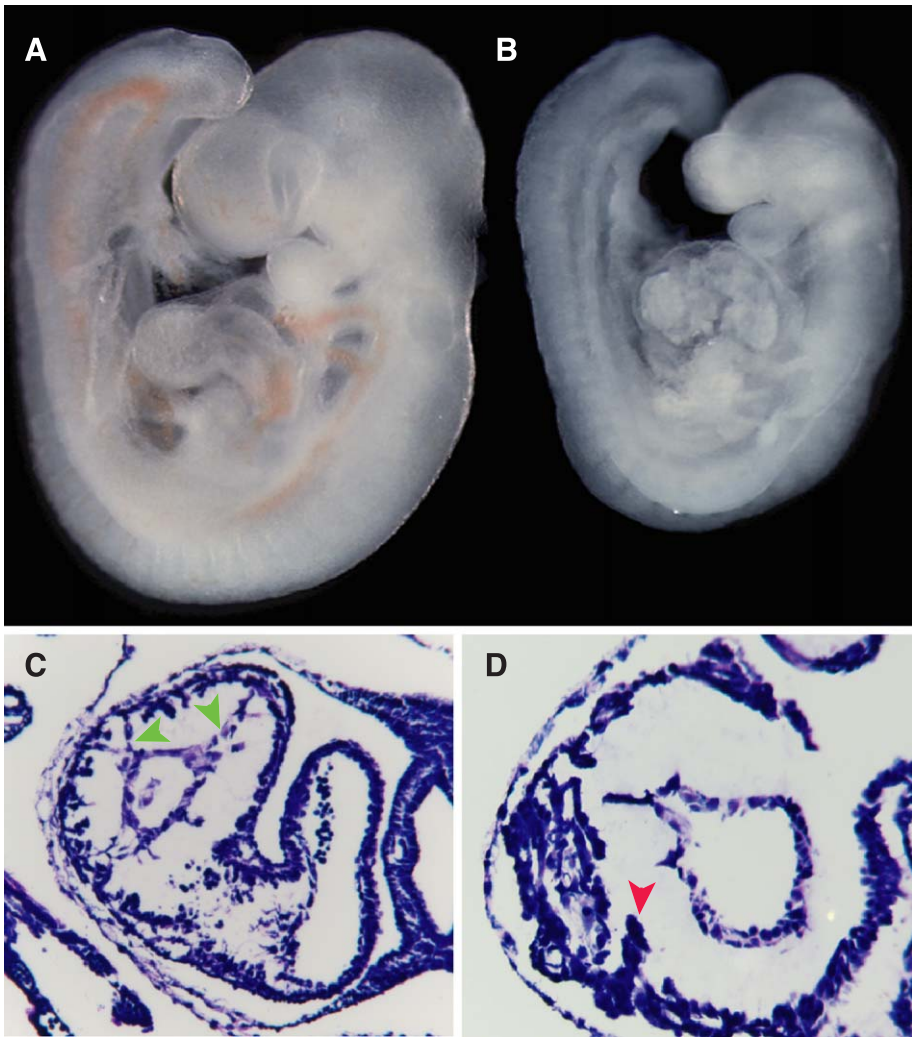

Fig. 2. Weakly contractile shru hearts had misaligned and abnormally shaped cardiomyocytes. When contrasted to wild-type (wt) (A), the *shru* heart (B) had a crinkled exterior appearance at 9.5 DPC. Sectioning of 8.75 DPC embryos revealed there are fewer trabeculae (green arrowheads) in mutant (D) than in wt (C) hearts. The red arrowhead in D indicates an abnormal clump of trabecular cells. Mutant myocardial and endocardial cells were misaligned with each other. Mutant cardiomyocytes had a cuboidal shape instead of the wild-type spindle shape.

the body. This failure of blood vessel integrity in mutant embryos indicated defective vascular development (Fig. 3H). The *shrunken-head* mutation causes lethality by 11.5 DPC, most likely because of the progression of these cardiovascular defects. Considering that the blood vessel defects and most of the increased cell death occur outside of *Titin*'s striated muscle expression, these components of the *shru* phenotype are likely to be a secondary result of cardiac dysfunction. It is noteworthy that *shru* embryos exhibit little variability in any aspect of their phenotype, indicating that absent circulation results in a specific and reproducible developmental deficit.

Regulation of angiogenesis is defective in shrunken-head embryos

The delayed onset of circulation in *shru* mutants provided the opportunity for a detailed investigation into the role of blood flow in vessel development. We first examined the extraembryonic vascular system in mutant embryos. Formation of the yolk sac vasculature involves both vasculogenesis and angiogenesis. An initial primitive vascular network of homogeneously sized vessels has been formed by 8.5 DPC via vasculogenic mechanisms. In wild-type embryos, angiogenic growth through sprouting and splitting of existing vessels combined with pruning and remodeling mechanisms had created a fractal network of large vitelline vessels and interconnecting fine capillaries by 9.5 DPC (Fig. 5A). Whole-mount and histological analyses of mutant yolk sacs at 8.5 DPC revealed no obvious abnormalities (data not shown). Angiogenesis defects were readily apparent by 9.5 DPC in the yolk sacs of shru embryos. Yolk sac blood vessels retained the primary vascular plexus architecture indicating little, if any, angiogenesis (Fig. 5B). This finding was confirmed via whole-mount PECAM-1 immunostaining (data not

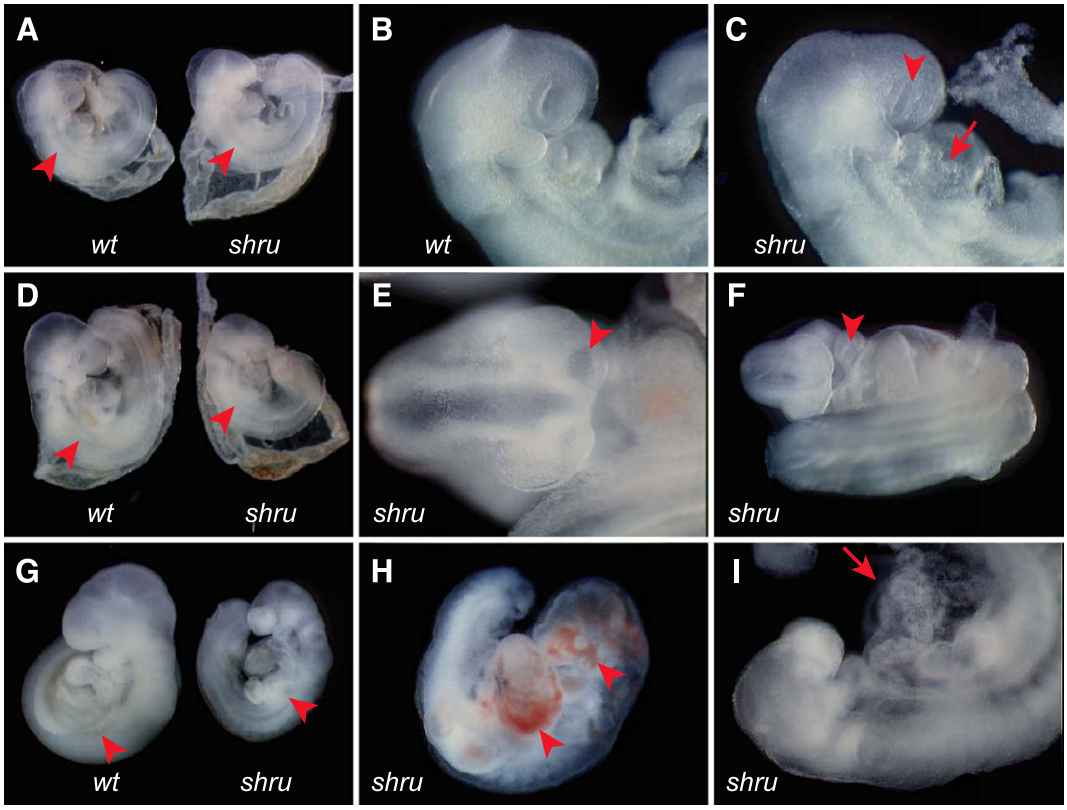

Fig. 3. Morphology of the shrunken-head phenotype. The first signs of the *shru* phenotype were apparent by 8.75 DPC (A–C). The optic vesicles were compressed along the anterior–posterior axis (arrowhead in C) when contrasted with wild-type (B). By 9.0 DPC (D–F), mutant embryos were growth retarded, but not developmentally delayed. At this stage, loss of cells in the frontonasal mesenchyme (arrowhead in E) and the first branchial arch (arrowhead in F) was visible. By 9.5 DPC (G–I), shru heads were markedly reduced in size. The absence of red blood cells along the dorsal aorta (arrowheads in A, D, and G) indicated vascular dysfunction in *shru* embryos. Mutants eventually developed hemorrhage (arrowheads in H) and progressively failing hearts (arrows in C and I).

shown). After 9.5 DPC, shru mutants did receive red blood cells in the vessels of the embryonic body axis. This demonstrates that there must have been at least some angiogenesis to connect the extraembryonic and embryonic vascular beds, which develop separately. By 10.5 DPC, *shru* yolk sacs appear avascular (data not shown), indicating that the extraembryonic blood vessels have been retracted.

To gain more insight into which cellular processes of angiogenesis are affected by the absence of blood flow, the vascular system of the embryo was examined in whole-mount from 8.8 to 9.2 DPC. Vessels were visualized using immunohistochemical detection of an antibody directed against the endothelial marker PECAM-1. The intersomitic vessels are some of the first embryonic vessels to form primarily by angiogenesis. ECs from the dorsal aortae project plasma membrane sprouts dorsally between the somites. These sprouting ECs then migrate towards the developing cardinal vein eventually forming fine capillary connections. The initial budding of intersomitic vessels appeared to occur normally in mutant embryos. Soon after these sprouts arose, they formed into abnormally dilated vessels (Fig. 5F).

Analysis of the vascular architecture at 9.0 DPC revealed other defects in angiogenesis. The dilated intersomitic vessels sprouted into aberrant locations, such as across or into somites (Fig. 5G). This resulted in abnormal connections between neighboring vessels. In addition, intersomitic capillaries later regressed completely, indicating excessive vascular pruning (Fig. 5H). Because the somites of *shru* mutants displayed increased cell death by 8.75 DPC, these intersomitic vessel defects could be attributed to loss of circulation, somitic cell death, or both. In other locations such as the head, the vasculature retained the primitive honeycomb pattern formed during vasculogenesis. There appeared to be minimal angiogenic growth, a lack of vascular remodeling, and possibly increased vessel fusion in the head (Fig. 5D).

Lack of circulation leads to abnormal endothelial shape, cell–cell contacts and cellular distribution

Local areas of hemorrhage developed in *shru* embryos once the delayed circulation began after 9.5 DPC. The failure of vessel integrity at 9.5 DPC as well as the widespread abnormalities in angiogenesis led us to specu-

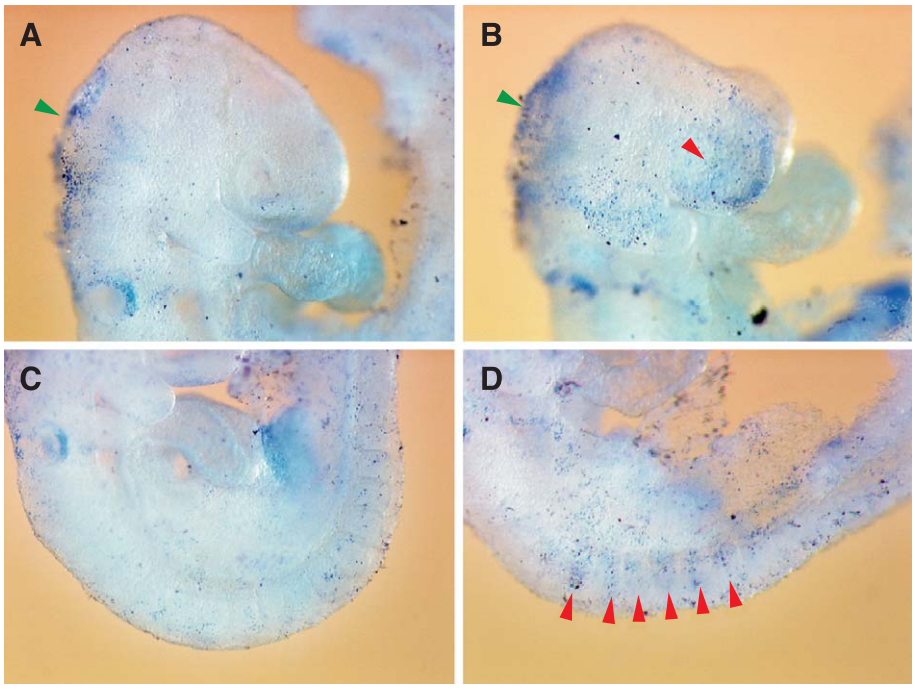

Fig. 4. Increased cell death preceded the loss of mesenchyme. Nile Blue Sulfate staining of 8.75 DPC embryos revealed increased cell death in *shru* mutants (B and D). Punctate blue staining marked normal areas (green arrowheads) of cell death such as the rhombencephalic roof and otic vesicles during development of wild-type embryos (A and C). Mutants had increased staining in the mesenchyme of the frontonasal mass and first branchial arch (red arrowhead in B) as well as in the somites (red arrowheads in D).

late that blood flow may play a prominent role in the maintenance and continued development of vasculogenic vessels in the embryo. We addressed the effect of absent circulation on the development of vasculogenic vessels by examining the dorsal aortae of 8.7 DPC embryos (Fig. 6). ECs comprising the dorsal aortae were identified in cross-sections using an antibody directed against PECAM-1. Quantification and visual analysis of these ECs revealed several distinct defects of vascular morphogenesis. A lumen was absent at many sites along the length of mutant vessels (Fig. 6E), despite the presence of PECAM-labeled ECs. In contrast, lumenal integrity was established throughout the length of the dorsal aortae in wild-type embryos. Sections in which mutant vessels lacked a clear lumen seemed to be associated with fewer PECAM-labeled ECs. This suggested either that ECs were mispositioned along the axis of the vessel or that there was an overall reduction in EC number. A comparison of the number of dorsal aorta ECs from serial sections indicated that the normal numbers of ECs were present in mutants (Fig. 7K). There was wide variation in the width of the mutant dorsal aortae in these sections. This abnormal width variation, which was also visible in whole-mount PECAM-labeled embryos (data not shown), seemed to occur randomly along the entire vessels. The variance in EC number between sections was significantly larger in mutant embryos, indicating that individual ECs were actually mispositioned along the A–P axis of these vessels. Analysis via whole-mount PECAM staining of the dorsal aortae as primitive ECs had just coalesced into vascular cords at 8.0 DPC indicated that the distribution of ECs at this time was normal (data not shown).

To search for a mechanistic cause(s) for these lumen formation and EC-distribution defects, the structure of mutant ECs in PECAM-labeled cross-sections was examined. The majority of embryonic cell types appeared to have normal shapes in sections of mutants. However, many ECs comprising the dorsal aortae in shru embryos had abnormal profiles. In contrast to the flattened profile of squamous wild-type ECs that have undergone spreading (Figs. 6A and C), mutant ECs tended to have a more globular profile (Figs. 6B, D, and F). Abnormal cellular protrusions that extended either apically or lumenally were visible in some mutant ECs. Several observations also demonstrate that cell–cell contacts were defective between mutant ECs. Wild-type ECs within a vessel make contact with their neighbors only along the edges of their flattened bodies. In contrast, extensive areas of cell–cell contact were seen between mutant ECs (Figs. 6E and F). The distribution of PECAM-1 staining on *shru* ECs also suggested defective cell–cell contact. In wild-type migrating angioblasts, PECAM-1 is uniformly distributed over the surface of the cell. Upon establishment of adheren junctions that lead up to lumenal morphogenesis, PECAM-1 is redistributed to the sites of contact (Fig. 6A and (Drake and Fleming, 2000)). In mutant ECs, PECAM-1 had a relatively widespread distribution, with limited concentration at areas of cell–cell apposition (Figs. 6B, E, and F).

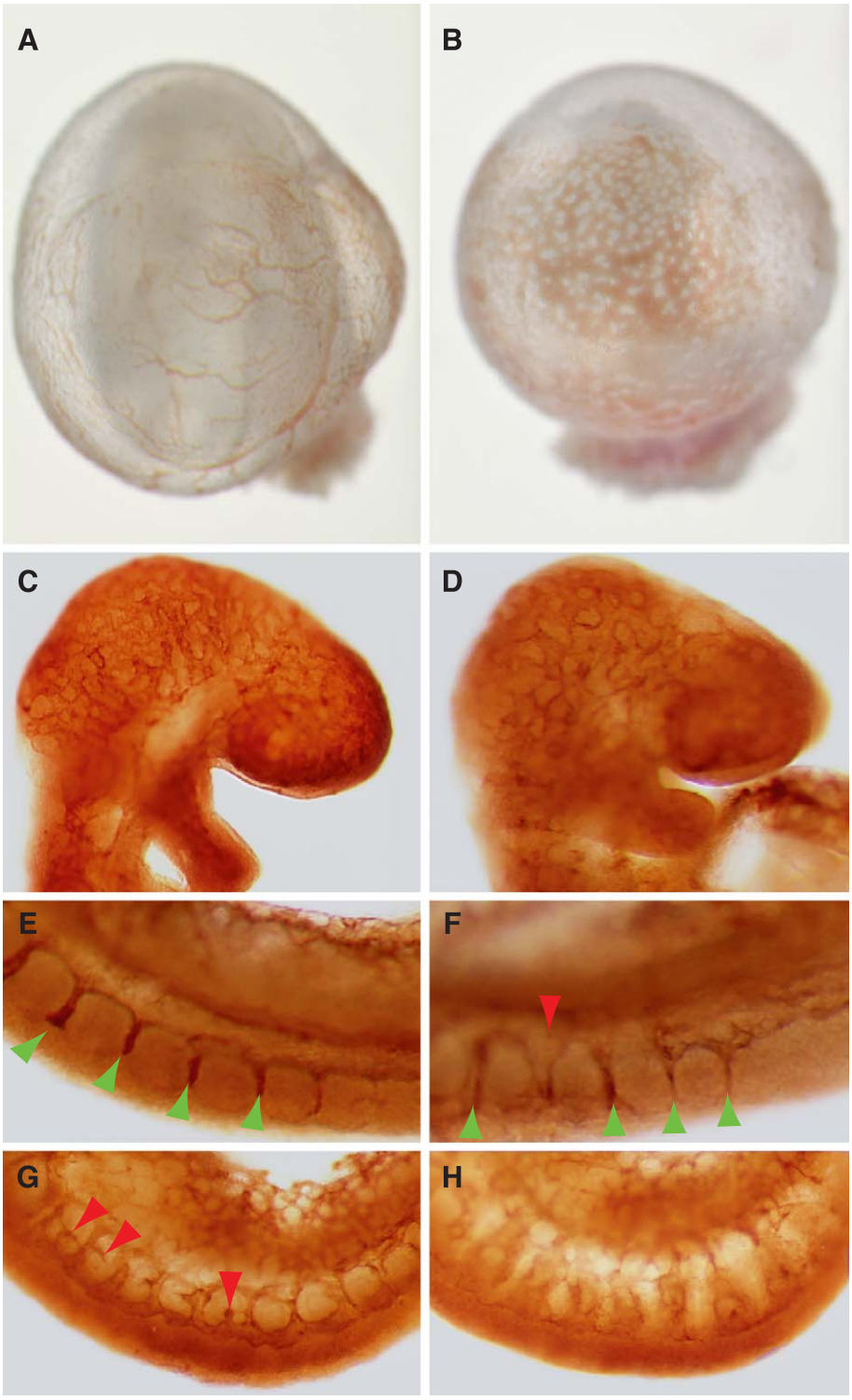

Fig. 5. Shru angiogenesis was limited and misregulated. By 9.5 DPC, angiogenesis had remodeled the wild-type (A) yolk sac vasculature into large and small caliber vessels. A mutant yolk sac at 9.5 DPC (B) retained the primitive vascular plexus pattern of homogeneously sized, large-bore vessels created during vasculogenesis. PECAM staining (C–H) revealed a more complex vascular network created by angiogenic sprouting and remodeling in a 9.0 DPC wt head (C). A 9.0 DPC *shru* head (D) showed dilated blood vessels with little sign of angiogenesis. At 8.8 DPC, angiogenic sprouting of the intersomitic vessels appeared relatively equivalent when comparing wt (E) and mutant (F) embryos (compare green arrowheads). The red arrowhead in F indicates an abnormally dilated vessel in the mutant. At 9.0 DPC in the mutant (G), PECAM-stained cells appear to extend abnormally into and around the somites (red arrowheads) originating from intersomitic vessels and the cardinal vein. Widespread vessel regression in the mutant at 9.2 DPC (H) resulted in the retraction of proper intersomitic vessels, but the aberrant somatic PECAM-stained cells remained.

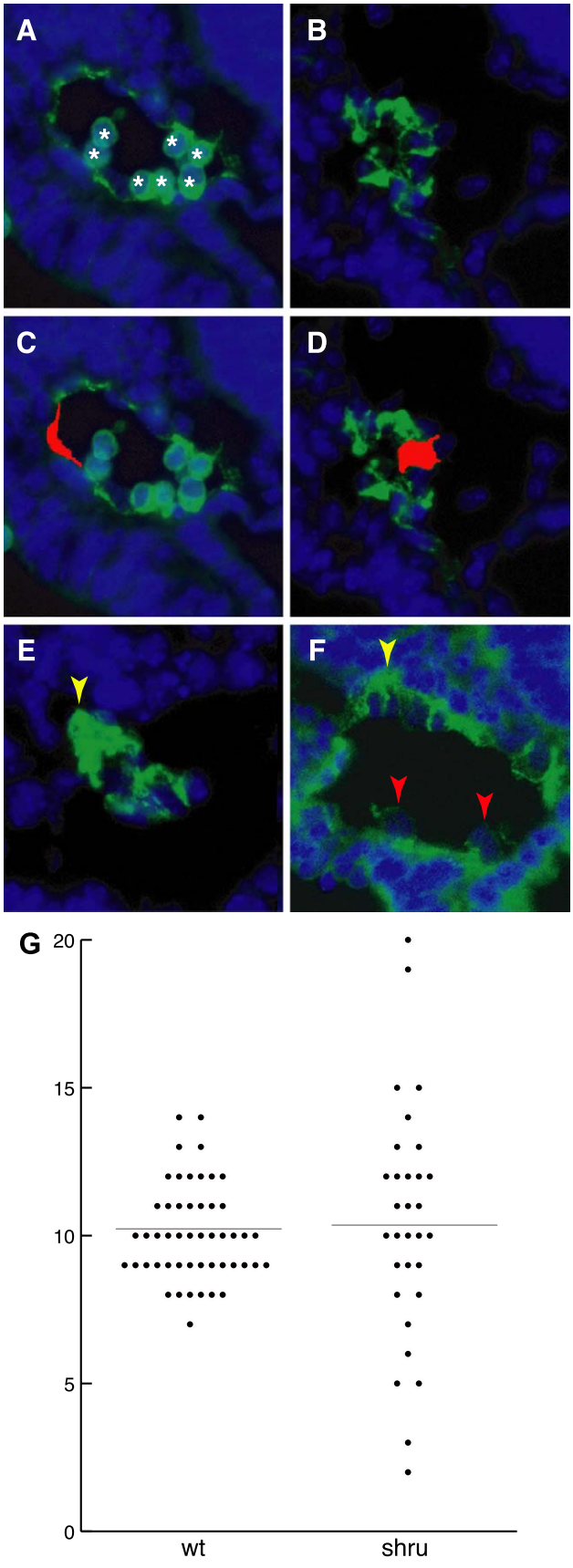

Increased VEGF signaling contributes to the shru phenotype

VEGF is a critical regulator of vascular morphogenesis. Several of the vascular defects seen in *shru* mutants such as the abnormal positioning and profiles of dorsal aortae ECs and increased vessel diameter resemble the effects of elevated VEGF signaling. VEGF expression is also known to be upregulated in response to hypoxia (Shweiki et al., 1992). The lack of circulation in *shru* mutants exposes embryos to the effects of hypoxia. Based on this, we investigated the role of VEGF in contributing to the defective vascular morphogenesis seen in *shru* mutants. Quantitative RT-PCR results indicated that VEGF-A expression was upregulated approximately 1.5- to 1.7-fold in *shru* mutants at 8.7 DPC (Fig. 7A). Assaying global mRNA expression using Affymetrix gene chips confirmed this result as VEGF expression was elevated 1.5-fold in 8.7 DPC mutants (data not shown).

Although VEGF is an extremely potent regulator of vascular development, the increased VEGF expression seen in *shru* mutants at 8.7 DPC was somewhat modest. We chose a genetic approach to determine if this elevated VEGF expression in *shru* mutants could be capable of affecting vascular development in vivo. We crossed a null allele of *Flt-1* (a receptor for VEGF) onto the *shrunken-head* mutant background. *Flt-1* is thought to serve an inhibitory role in VEGF signaling. Reduction of *Flt-1* function would likely exacerbate any affects that elevated VEGF signaling was having on the endothelial cell defects in *shru*.

The null allele of *Flt-1* used (Flt-1 LacZ) was created by replacing part of its coding sequence with that of the LacZ gene (Fong et al., 1995), providing a useful histochemical marker for the endothelium. Examination of the vasculature

Fig. 6. Defective endothelial shape, cell–cell contacts, and mispositioning of ECs in shrunken-head mutants. PECAM-1 immunofluorescence (green) and Hoechst staining of nuclei (blue) from 10-μm transverse sections were used to visualize a cross-section of right dorsal aorta from 12-somite embryos (panels A–F). In a wild-type embryo (A), the lumen of the dorsal aorta was filled with cylindrical red blood cells (marked with *). In panel C, a wild-type endothelial cell has been shaded red to illustrate the thin profile typical to the simple squamous epithelium of a vessel. Many mutant ECs (B, D, and F) possessed a thick profile. A *shru* EC shaded in red (D) had abnormal apical and lumenal plasma membrane protrusions. Aberrant cellular profiles and lumenal plasma membrane protrusions in *shru* mutant ECs are also shown in F (red arrowheads). Mutant ECs in the dorsal aorta (E) also displayed defective cell–cell contacts, making contact with each other along large extents of their cell surfaces. The failure of PECAM-1 staining to be redistributed to sites of cell contact (yellow arrowheads in E and F) is consistent with defective cell–cell contacts in mutant ECs. A clear vascular lumen was absent in many mutant sections (E). ECs exhibited a scattered distribution along the anterior–posterior axis in *shru* mutants. Scatter plots show the number of ECs forming each side of the dorsal aorta per section in wt and shru (G). The mean number of ECs between wt and mutant did not differ significantly (see Fig. 7K), but the variance (s^2) was substantially higher in *shru* (s^2: 15.60) than wt (s^2: 2.60), indicating cells were mispositioned.

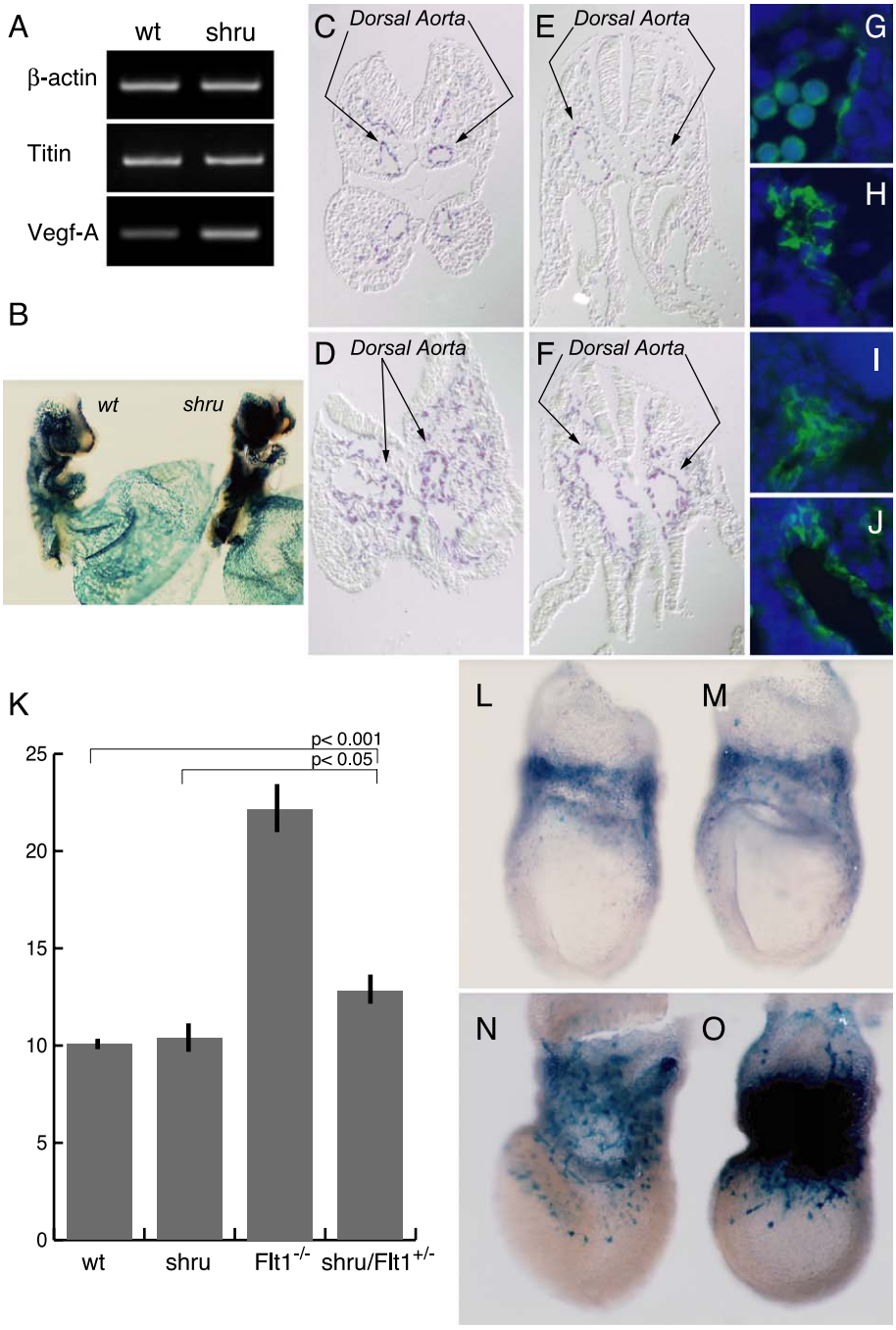

Fig. 7. Increased VEGF signaling likely contributes to vascular defects in shru. (A) Quantitative RT-PCR indicated elevated VEGF-A expression in shru mutants at 8.75 DPC. The *shrunken-head* mutation also genetically interacted with Flt-1 to regulate EC number (B–K). A flt-shru mutant showed much stronger staining of the Flt-1 LacZ knock-in reporter than wt at 8.75 DPC (B). Transverse sections of these LacZ-stained embryos revealed elevated numbers of Flt-1-expressing cells scattered throughout the mesenchyme of the flt-shru mutant (D and F) compared to the wild-type vasculature of the *flt-1*+/− embryo (C and E). Vasculogenic vessels in flt-shru mutants had abnormally large lumens with ectopic clusters of Flt-1-expressing cells inside the lumens. PECAM-1 staining in the dorsal aortae was used to quantitate the increased number of ECs in flt-shru embryos. Transverse sections from 11 to 13 somite embryos were immunofluorescently labeled using a PECAM-1 antibody (green). Nuclei (blue) were counterstained with Hoechst. Wild-type (G) and *shru*−/− (H) showed similar numbers of ECs. Sections from a flt-shru mutant (I) and a *flt-1*−/− mutant (J) revealed an increase in EC number. The number of ECs comprising a 10-μm section of dorsal aorta is shown in K. The mean number of ECs does not differ significantly between wild-type and *shru* (bars indicate SEM). The increase in ECs seen in flt-shru mutants is significant ($P < 0.05$), but not as large as the increase of ECs in *flt-1*−/− mutants. Flt-1 LacZ staining appeared equivalent in a wt (L) and a flt-shru mutant (M) at 7.4 DPC, indicating similar numbers of angioblasts. However, a *flt-1*−/− mutant (O) had a clear increase in angioblast number compared to wt (N) at 7.5 DPC.

in all possible genetic combinations revealed an obvious interaction in 8.75 DPC embryos heterozygous for Flt-1 LacZ and homozygous for *shru* (called flt-shru embryos hereafter). Whole-mount staining for β-gal in flt-shru embryos at 8.75 DPC showed an excess of flt-1-expressing cells and vascular disorganization throughout flt-shru embryos (Fig. 7B). Embryos heterozygous for the *Flt-1* mutation possess a wild-type vasculature with no detectable increase in EC number compared to wild-type embryos (Figs. 7C and E and Fong et al., 1999). Sections of flt-shru mutants showed increased numbers of Flt-1-expressing cells comprising major vessels such as the dorsal aortae and the anterior cardinal veins (Figs. 7D and F). These vessels had enlarged lumens and ectopic Flt-1-expressing cells within the lumen. Abnormal clusters of labeled cells were also scattered throughout the mesenchyme. These characteristics of flt-shru mutants appeared identical to that reported for *Flt-1* homozygotes (Fong et al., 1995).

The presence of ectopic Flt-1-expressing cells in flt-shru embryos raised the question of whether the flt-shru phenotype indicated an overproduction of ECs or merely aberrant Flt-1 expression. Ectopic cells within the lumens of the dorsal aortae of flt-shru embryos were determined to be PECAM-1-expressing ECs (Fig. 7I). A comparison of EC number from these PECAM-labeled sections indicated that flt-shru mutants have significantly more ECs compared to *shru*−/− or wt embryos, but this increase was not as great as in *Flt-1*−/− mutants (Fig. 7K). This genetic interaction between *Flt-1* and *shru* indicates that the elevated VEGF expression characterized here can affect blood vessel development in vivo and likely contributes to the endothelial defects seen in *shru* mutants.

The developmental basis for the vascular defects in flt-1 homozygotes has been traced back to an excessive number of endothelial precursors at 7.0 DPC (Fong et al., 1999). However, there was no detectable difference in the number of ECs and precursors in flt-shru embryos versus *Flt-1* heterozygotes when assayed between 7.4 and 8.25 DPC (Figs. 7L and M and data not shown). The increase in the EC population in *flt-shru* mutants is detectable at 8.5 DPC (data not shown). This genetic interaction reveals a new role for *Flt-1* in regulating EC number after lumenization of blood vessels.

Discussion

The *shrunken-head* mutation produces a complex set of developmental malformations, including cardiovascular deficits and increased death of specific cell types. Localization of the shru mutation within the *Titin* gene has revealed new roles for Titin in heart development and has yielded important insights into the role of circulation in vascular morphogenesis and maintenance of particular mesenchymal cell types.

Titin controls the alignment and shape of cardiac cells

A large body of evidence exists supporting structural roles for Titin filaments in cardiac and skeletal muscles (Gregorio et al., 1999). The *Titin* locus encodes single polypeptides that can be over 3 MDa which are quite modular in structure. Single Titin polypeptides have been shown to span half the sarcomere from the Z-disc to the M-line. Titins are believed serve as blueprints for sarcomere assembly; aligning other structural, regulatory, and contractile proteins within the sarcomere via direct protein–protein interactions. In this manner, Titin coordinates the precisely arranged assembly of myofibrils into more complex sarcomeric structures in striated muscle (van der Ven et al., 2000). By serving as a molecular spring, Titin has also been shown to maintain the structural integrity of contracting myofibrils. These spring-like features of Titin polypeptides provide muscle fibers with passive elasticity (Labeit and Kolmerer, 1995; Linke et al., 2002). The *Titin* locus is subject to complex transcriptional regulation and alternative splicing. The use of alternative 3′ termini and the inclusion or exclusion of particular exons produce diverse Titin products with different myofibril assembly and elasticity properties (Bang et al., 2001; Freiburg et al., 2000). Considering Titin's structural roles in striated muscle, it is not surprising that the *shru* mutation produces an embryonic lethal cardiovascular phenotype. The nature of this phenotype reveals new roles for *Titin* in regulating the alignment and shape of developing cardiomyocytes.

The *shru* mutation produces poor contractility of the embryonic heart and delays the onset of circulation by more than a day. Despite this lack of circulation, cardiac morphogenesis and the pattern formation are not affected in *shru* mutants, indicating that proper heart function is not required for these developmental processes. *Shru* hearts are weakly contractile from the outset, indicating that at least some elements of the cardiac contractile apparatus are assembled. In the mouse heart, Titin expression begins at 7.75 DPC, preceding myofibril assembly. Mutations in *Titin* have been shown to cause dilated cardiomyopathy in humans, zebrafish, and the mouse (Gerull et al., 2002; Gotthardt et al., 2003; Xu et al., 2002). In the zebrafish mutant *pik*^{m171}, loss of Titin function in the heart reduces the number of myofibrils and severely limits contractility of the heart. In addition, loss of muscle elasticity can be seen in individual cardiomyocytes as they become thin and bulge outwards after contraction has begun. *Shru* hearts do not possess a dilated cardiomyopathy phenotype. Instead, cells in the myocardium and endocardium are cuboidal and misaligned. The aberrant cuboidal shape seen in shru cardiomyocytes could result from problems in myofibril assembly or a defective cytoskeleton. Interestingly, the cellular defects in shru hearts closely resemble those seen in hearts null for *Mef2c* (Bi et al., 1999) or *N-cadherin* (Luo et al., 2001; Radice et al., 1997). The fact that myocardial cells that form trabeculae are also misaligned makes it less

clear how defective myofibrils could account for the cellular defects seen in shru hearts. Given the differences between *shru* hearts and those with previously documented *Titin* mutations, it seems likely that *shru* is a hypomorphic allele that does not abolish muscle elasticity. This could explain why *shru* cardiomyocytes do not appear to stretch out excessively as in zebrafish *pickwick* mutants. The *shru* mutation does not alter *Titin*'s mRNA expression pattern or levels. Because *shru* was induced by ENU, it is most likely a point mutation distal to the N2B region of I-band Titin that either creates a nonsense or missense codon, or alters a splice donor or acceptor site.

Titin and cell death

In addition to those mutations that cause dilated cardiomyopathy, other documented mutations in mouse and human *Titin* cause muscular dystrophy in the adult (Garvey et al., 2002; Hackman et al., 2002). This progressive breakdown and loss of certain skeletal muscle tissue is thought to result from sarcomeric instability. However, none of the other *Titin* mutations have been shown to cause cell death in the developing somites, the precursors to skeletal muscle and bone. *Shru* embryos display distinct areas of increased cell death at 8.75 DPC, including the sclerotomal precursor regions of the somites. Titin expression begins in the somites at 8.25 DPC even though skeletal muscle contractions do not begin until many days later in gestation. Elevated cell death within mutant somites could indicate a local role for *Titin* in preventing cell death or could be a secondary result of the cardiac defects.

Complete circulatory insufficiency appears to cause widespread death from hypoxia in virtually all cell types at 9.5 DPC. *Shru* embryos have increased levels of cell death in specific cell populations of the head evident at 8.75 DPC. These regions, the frontonasal mass and the first branchial arch, are all comprised of mesenchymal cell types. Because these areas of the embryo do not express *Titin*, we believe this specific pattern of cell death is the result of cardiac dysfunction. Mutations in the BMP signaling mediator *Smad5*, the GTPase-activating protein *p120-rasGAP*, and the serine–threonine kinase *Lkb1* produce a similar pattern of cell death coincident with apparent cardiac dysfunction (Henkemeyer et al., 1995; Yang et al., 1999; Ylikorkala et al., 2001). However, these mutations produce a variety of developmental defects so it is difficult to assess the role of cardiovascular function in maintaining these cells. A null mutation in *Ncx1* produces embryos that lack a heartbeat and embryonic blood circulation (Koushik et al., 2001). *Ncx1* is a sodium–calcium exchanger expressed exclusively in the heart up to 11.0 DPC. Defects seen in these embryos outside of the heart are believed to result from lack of cardiac function. The first branchial arch of 9.5 DPC *Ncx1*−/− mice is hollow and hypoplastic, indicating a loss of this cell population (Conway et al., 2003). This closely resembles the pharyngeal arch in *shru* embryos. The frontonasal region of *Ncx1*−/− mice has not been examined closely to determine if it also exhibits the cell death pattern that characterizes *shru* embryos. We believe that cells in the first branchial arch and frontonasal mesenchyme die prematurely in *shru* embryos because they are either more affected by hypoxia than other tissues or that cardiovascular failure produces aberrant signaling leading to increased apoptosis. The head mesenchyme of wild-type embryos shows evidence of hypoxia by 8.5 DPC (Lee et al., 2001). This could indicate why these cells appear to be some of the first to die after failure to establish embryonic circulation.

Biomechanical forces direct vascular morphogenesis

Shrunken-head embryos display various morphogenic defects during vessel development. In the yolk sac, vasculogenesis appears to occur normally, but the resulting primitive vascular network does not undergo angiogenic remodeling. In the embryo itself, angiogenesis is reduced and its spatial regulation is abnormal. Vessels within the embryo do not maintain the integrity of vascular lumens. At the cellular level, *shrunken-head* ECs have defects in their shape, their position, and in interactions with their neighboring cells. Because the primary effect of the *shru* mutation is to disrupt Titin function and alter contractility of the heart, this provides an opportunity to understand how the lack of circulation affects the cellular and network aspects of vascular morphogenesis.

Ordinarily, endothelial precursors migrate to the site of vasculogenesis and interact with other endothelial cells through cell–cell contacts to form the primary vascular plexus. Continued interaction between endothelial cells allows this plexus to coalesce into a set of tubes. During the transition from migration to tubulogenesis, endothelial cells undergo dramatic cell shape changes. Migrating cells have relatively compact cell bodies with directionally extended cell processes leading the migration. As they interact with their fellows to form the vasculature, they adopt a squamous shape. Endothelial precursors are believed to mediate the beginning stages of vasculogenesis through biochemical regulation of their cellular behaviors. Contraction of the heart begins soon after the first vessels of the primary vascular plexus have lumenized. As soon as heart contractions begin, endothelial cells that are forming the vasculature are subjected to new biomechanical stimuli from circulation. These include hydrostatic pressures, fluid shear stresses, and cyclic strains. We believe that the lack of biomechanical stimuli from absent circulation produces many of the specific vascular morphogenic defects seen in *shru* endothelial cells. In this context, fluid biomechanical forces produced from the very onset of cardiac contractions are required to direct vascular morphogenesis and endothelial differentiation in vivo.

A large body of evidence indicates that hemodynamic forces profoundly influence the phenotype of ECs in vitro (Topper and Gimbrone, 1999). ECs in culture show

distinct responses to fluid shear stresses that include changes in gene transcription, cell shape alterations, directional migration, and various alterations in metabolic and synthetic activities. Of interest in relation to the *shru* phenotype, ECs exposed in culture to steady laminar shear stresses reproducibly elongate and align their axes in the direction of flow (Galbraith et al., 1998). Reorganization of actin-containing stress fibers begins within minutes of exposure to this form of stimulus (Birukov et al., 2002). ECs also migrate away from the source of steady laminar flow. While much progress has been made in defining how biomechanical stimuli alter EC phenotype in vitro and which cellular molecules transduce these effects, many of these models have not been tested in vivo.

Dynamic responses of blood vessels to hemodynamic forces have been demonstrated in studies of the yolk sac vasculature. After experimentally altering the pathway of blood flow, yolk sac vessels begin retraction of superfluous vessels and angiogenic growth and reorganization of new vessels within minutes. It has become clear that circulation is indeed required for angiogenesis within the yolk sac (Koushik et al., 2001; Luo et al., 2001), and the study of *shru* confirms that. Within the embryo, angiogenic growth of some vessels follows a genetic program while others are shaped primarily by the particular metabolic demands of neighboring tissues (Graef et al., 2001). We demonstrate that many of the cellular mechanisms of angiogenesis such as sprouting and vessel interconnection and retraction are preserved in the absence of circulation. However, an intact circulation seems to be necessary to spatially direct these cellular processes during vessel growth and reorganization.

In contrast to angiogenesis, vasculogenic development begins before the onset of blood flow. Study of the biochemical regulation of vasculogenesis has identified several molecules that when mutated disrupt vasculogenic development (for a review, see Sato, 1999). Vessels created during vasculogenesis begin to exhibit defects after circulation has been delayed in *shru* mutants. After the alignment of primordial ECs at the vertices of future vessels and cell–cell contact formation to create a lumen, shru ECs do not assume the flattened, squamous shape typical of the endothelial differentiation pathway. Instead, *shru* ECs retain several characteristics resembling the more primitive state of migrating angioblasts, such as noticeable plasma membrane protrusions. This may indicate that *shru* ECs can lose their apical–lumenal polarity acquired during vasculogenesis. Given the presence of these membrane protrusions which angioblast use to migrate, we believe that *shru* ECs comprising vessels migrate abnormally to create the uneven distribution of cells seen along the vessel's length. This proposed migration defect coupled with abnormal cell–cell contacts could lead to the disrupted lumenal integrity of blood vessels in shru mutants. We conclude that biomechanical forces produced from circulation are required to maintain vascular lumen integrity after vasculogenesis and direct the functional phenotype of ECs by influencing their shape and cell–cell contacts. The effects of hemodynamic forces on ECs observed in vitro appear to be critical components of early vessel morphogenesis in vivo.

Role of VEGF in shru mutants

VEGF is a critical regulator of several aspects of vascular morphogenesis. VEGF regulates migration by functioning as a chemoattractant for ECs. Increasing endogenous amounts of VEGF results in increased vessel fusion and elevated protrusive activity of EC plasma membranes (Drake and Little, 1995; Drake et al., 2000). The vascular defects seen in *shru* mutants resemble effects described from increasing endogenous levels of VEGF, and indeed *shru* mutants have increased expression of VEGF-A mRNA shortly following the delay in circulation. *Shru* mutants eventually develop dilated vessels in the head, and ECs possess abnormal plasma membrane protrusions and an abnormal distribution within vessels. A genetic interaction between the *shru* mutation and a null mutation in *Flt-1* produces an increase in endothelial cell number in flt-shru embryos, thus reinforcing that the increased VEGF expression at 8.7 DPC could influence vascular development. Although significant, this increase in EC number was not as large as that seen in *Flt-1*−/− mice. We interpret this relatively weak genetic interaction to result from elevated VEGF activity in *shru* mutants, rather than as evidence that Titin and Flt-1 proteins might physically interact. Given that expression of VEGF is elevated in response to hypoxia, it is not surprising that absent circulation in *shru* mutants would increase VEGF levels. This is the earliest time point that VEGF activity has been shown to be elevated following cardiac defects. Considering VEGF's defined roles in vascular development, it is possible that aspects of the *shru* vascular phenotype result from altered VEGF signaling rather than from a response to biomechanical stimuli. Interestingly, in zebrafish mutants such as *island beat* which prevent blood circulation, VEGF expression remains normal and early vascular development proceeds unimpeded (Serluca et al., 2002). Although these mutants lack vascular growth in some areas such as in the kidney, ECs within vasculogenic vessels appear to form normal cellular junctions.

The genetic interaction between *Flt-1* and *shru* also uncovered a new role for *Flt-1* in regulating EC number. It is clear from the timing of this interaction that *Flt-1* continues to regulate EC number after lumenization of blood vessels. It is not evident whether this is accomplished by affecting EC proliferation or continued recruitment mesodermal angioblasts.

References

Bang, M.L., Centner, T., Fornoff, F., Geach, A.J., Gotthardt, M., McNabb, M., Witt, C.C., Labeit, D., Gregorio, C.C., Granzier, H., et al., 2001. The complete gene sequence of titin, expression of an unusual approximately 700-kDa titin isoform, and its interaction with

obscurin identify a novel Z-line to I-band linking system. Circ. Res. 89, 1065–1072.
Bennett, H.S., Wyrick, A.D., Lee, S.W., McNeil, J.H., 1976. Science and art in preparing tissues embedded in plastic for light microscopy, with special reference to glycol methacrylate, glass knives and simple stains. Stain Technol. 51, 71–97.
Bi, W., Drake, C.J., Schwarz, J.J., 1999. The transcription factor MEF2C-null mouse exhibits complex vascular malformations and reduced cardiac expression of angiopoietin 1 and VEGF. Dev. Biol. 211, 255–267.
Birukov, K.G., Birukova, A.A., Dudek, S.M., Verin, A.D., Crow, M.T., Zhan, X., DePaola, N., Garcia, J.G., 2002. Shear stress-mediated cytoskeletal remodeling and cortactin translocation in pulmonary endothelial cells. Am. J. Respir. Cell Mol. Biol. 26, 453–464.
Carmeliet, P., Mackman, N., Moons, L., Luther, T., Gressens, P., Van Vlaenderen, I., Demunck, H., Kasper, M., Breier, G., Evrard, P., et al., 1996. Role of tissue factor in embryonic blood vessel development. Nature 383, 73–75.
Cleaver, O., Krieg, P.A., 1998. VEGF mediates angioblast migration during development of the dorsal aorta in *Xenopus*. Development 125, 3905–3914.
Coan, D.E., Wechezak, A.R., Viggers, R.F., Sauvage, L.R., 1993. Effect of shear stress upon localization of the Golgi apparatus and microtubule organizing center in isolated cultured endothelial cells. J. Cell Sci. 104 (Pt. 4), 1145–1153.
Coffin, J.D., Poole, T.J., 1991. Endothelial cell origin and migration in embryonic heart and cranial blood vessel development. Anat. Rec. 231, 383–395.
Conway, S.J., Kruzynska-Frejtag, A., Kneer, P.L., Machnicki, M., Koushik, S.V., 2003. What cardiovascular defect does my prenatal mouse mutant have, and why? Genesis 35, 1–21.
de Vries, C., Escobedo, J.A., Ueno, H., Houck, K., Ferrara, N., Williams, L.T., 1992. The fms-like tyrosine kinase, a receptor for vascular endothelial growth factor. Science 255, 989–991.
Dewey Jr., C.F., Bussolari, S.R., Gimbrone Jr., M.A., Davies, P.F., 1981. The dynamic response of vascular endothelial cells to fluid shear stress. J. Biomech. Eng. 103, 177–185.
Dietrich, W.F., Copeland, N.G., Gilbert, D.J., Miller, J.C., Jenkins, N.A., Lander, E.S., 1995. Mapping the mouse genome: current status and future prospects. Proc. Natl. Acad. Sci. U. S. A. 92, 10849–10853.
Drake, C.J., Fleming, P.A., 2000. Vasculogenesis in the day 6.5 to 9.5 mouse embryo. Blood 95, 1671–1679.
Drake, C.J., Little, C.D., 1995. Exogenous vascular endothelial growth factor induces malformed and hyperfused vessels during embryonic neovascularization. Proc. Natl. Acad. Sci. U. S. A. 92, 7657–7661.
Drake, C.J., Little, C.D., 1999. 1 the de novo formation of blood vessels. J. Histochem. Cytochem. 47, 1643.
Drake, C.J., Hungerford, J.E., Little, C.D., 1998. Morphogenesis of the first blood vessels. Ann. N. Y. Acad. Sci. 857, 155–179.
Drake, C.J., LaRue, A., Ferrara, N., Little, C.D., 2000. VEGF regulates cell behavior during vasculogenesis. Dev. Biol. 224, 178–188.
Ferrara, N., 1999. Molecular and biological properties of vascular endothelial growth factor. J. Mol. Med. 77, 527–543.
Fong, G.H., Rossant, J., Gertsenstein, M., Breitman, M.L., 1995. Role of the Flt-1 receptor tyrosine kinase in regulating the assembly of vascular endothelium. Nature 376, 66–70.
Fong, G.H., Zhang, L., Bryce, D.M., Peng, J., 1999. Increased hemangioblast commitment, not vascular disorganization, is the primary defect in flt-1 knock-out mice. Development 126, 3015–3025.
Frame, M.D., Sarelius, I.H., 2000. Flow-induced cytoskeletal changes in endothelial cells growing on curved surfaces. Microcirculation 7, 419–427.
Freiburg, A., Trombitas, K., Hell, W., Cazorla, O., Fougerousse, F., Centner, T., Kolmerer, B., Witt, C., Beckmann, J.S., Gregorio, C.C., et al., 2000. Series of exon-skipping events in the elastic spring region of titin as the structural basis for myofibrillar elastic diversity. Circ. Res. 86, 1114–1121.
Galbraith, C.G., Skalak, R., Chien, S., 1998. Shear stress induces spatial reorganization of the endothelial cell cytoskeleton. Cell Motil. Cytoskeleton 40, 317–330.
Garvey, S.M., Rajan, C., Lerner, A.P., Frankel, W.N., Cox, G.A., 2002. The muscular dystrophy with myositis (mdm) mouse mutation disrupts a skeletal muscle-specific domain of titin. Genomics 79, 146–149.
Gerull, B., Gramlich, M., Atherton, J., McNabb, M., Trombitas, K., Sasse-Klaassen, S., Seidman, J.G., Seidman, C., Granzier, H., Labeit, S., et al., 2002. Mutations of TTN, encoding the giant muscle filament titin, cause familial dilated cardiomyopathy. Nat. Genet. 30, 201–204.
Gluzman-Poltorak, Z., Cohen, T., Herzog, Y., Neufeld, G., 2000. Neuropilin-2 is a receptor for the vascular endothelial growth factor (VEGF) forms VEGF-145 and VEGF-165. J. Biol. Chem. 275, 29922.
Gotthardt, M., Hammer, R.E., Hubner, N., Monti, J., Witt, C.C., McNabb, M., Richardson, J.A., Granzier, H., Labeit, S., Herz, J., 2003. Conditional expression of mutant M-line titins results in cardiomyopathy with altered sarcomere structure. J. Biol. Chem. 278, 6059–6065.
Graef, I.A., Chen, F., Chen, L., Kuo, A., Crabtree, G.R., 2001. Signals transduced by Ca(2+)/calcineurin and NFATc3/c4 pattern the developing vasculature. Cell 105, 863–875.
Gregorio, C.C., Granzier, H., Sorimachi, H., Labeit, S., 1999. Muscle assembly: a titanic achievement? Curr. Opin. Cell Biol. 11, 18–25.
Hackman, P., Vihola, A., Haravuori, H., Marchand, S., Sarparanta, J., De Seze, J., Labeit, S., Witt, C., Peltonen, L., Richard, I., et al., 2002. Tibial muscular dystrophy is a titinopathy caused by mutations in TTN, the gene encoding the giant skeletal-muscle protein titin. Am. J. Hum. Genet. 71, 492–500.
Henkemeyer, M., Rossi, D.J., Holmyard, D.P., Puri, M.C., Mbamalu, G., Harpal, K., Shih, T.S., Jacks, T., Pawson, T., 1995. Vascular system defects and neuronal apoptosis in mice lacking ras GTPase-activating protein. Nature 377, 695–701.
Hentges, K., Thompson, K., Peterson, A., 1999. The flat-top gene is required for the expansion and regionalization of the telencephalic primordium. Development 126, 1601–1609.
Hogan, B., Beddington, R., Costantini, F., Lacy, E., 1994. Manipulating the Mouse Embryo: A Laboratory Manual. Cold Spring Harbor Laboratory Press, New York.
Koushik, S.V., Wang, J., Rogers, R., Moskophidis, D., Lambert, N.A., Creazzo, T.L., Conway, S.J., 2001. Targeted inactivation of the sodium-calcium exchanger (Ncx1) results in the lack of a heartbeat and abnormal myofibrillar organization. FASEB J. 15, 1209–1211.
Labeit, S., Kolmerer, B., 1995. Titins: giant proteins in charge of muscle ultrastructure and elasticity. Science 270, 293–296.
Lee, Y.M., Jeong, C.H., Koo, S.Y., Son, M.J., Song, H.S., Bae, S.K., Raleigh, J.A., Chung, H.Y., Yoo, M.A., Kim, K.W., 2001. Determination of hypoxic region by hypoxia marker in developing mouse embryos in vivo: a possible signal for vessel development. Dev. Dyn. 220, 175–186.
Li, S., Butler, P., Wang, Y., Hu, Y., Han, D.C., Usami, S., Guan, J.L., Chien, S., 2002. The role of the dynamics of focal adhesion kinase in the mechanotaxis of endothelial cells. Proc. Natl. Acad. Sci. U. S. A. 99, 3546–3551.
Linke, W.A., Kulke, M., Li, H., Fujita-Becker, S., Neagoe, C., Manstein, D.J., Gautel, M., Fernandez, J.M., 2002. PEVK domain of titin: an entropic spring with actin-binding properties. J. Struct. Biol. 137, 194–205.
Luo, Y., Ferreira-Cornwell, M., Baldwin, H., Kostetskii, I., Lenox, J., Lieberman, M., Radice, G., 2001. Rescuing the N-cadherin knockout by cardiac-specific expression of N- or E-cadherin. Development 128, 459–469.
Miquerol, L., Gertsenstein, M., Harpal, K., Rossant, J., Nagy, A., 1999. Multiple developmental roles of VEGF suggested by a LacZ-tagged allele. Dev. Biol. 212, 307–322.
Plouet, J., Schilling, J., Gospodarowicz, D., 1989. Isolation and characterization of a newly identified endothelial cell mitogen produced by AtT-20 cells. EMBO J. 8, 3801–3806.
Radice, G.L., Rayburn, H., Matsunami, H., Knudsen, K.A., Takeichi, M., ,

Hynes, R.O., 1997. Developmental defects in mouse embryos lacking N-cadherin. Dev. Biol. 181, 64–78.

Risau, W., Lemmon, V., 1988. Changes in the vascular extracellular matrix during embryonic vasculogenesis and angiogenesis. Dev. Biol. 125, 441–450.

Sato, T.N., 1999. Gene trap, gene knockout, gene knock-in, and transgenics in vascular development. Thromb. Haemostasis 82, 865–869.

Schaart, G., Viebahn, C., Langmann, W., Ramaekers, F., 1989. Desmin and titin expression in early postimplantation mouse embryos. Development 107, 585–596.

Serluca, F.C., Drummond, I.A., Fishman, M.C., 2002. Endothelial signaling in kidney morphogenesis: a role for hemodynamic forces. Curr. Biol. 12, 492–497.

Shweiki, D., Itin, A., Soffer, D., Keshet, E., 1992. Vascular endothelial growth factor induced by hypoxia may mediate hypoxia-initiated angiogenesis. Nature 359, 843–845.

Soker, S., Takashima, S., Miao, H.Q., Neufeld, G., Klagsbrun, M., 1998. Neuropilin-1 is expressed by endothelial and tumor cells as an isoformspecific receptor for vascular endothelial growth factor. Cell 92, 735–745.

Sugi, Y., Markwald, R.R., 1996. Formation and early morphogenesis of endocardial endothelial precursor cells and the role of endoderm. Dev. Biol. 175, 66–83.

Suri, C., Jones, P.F., Patan, S., Bartunkova, S., Maisonpierre, P.C., Davis, S., Sato, T.N., Yancopoulos, G.D., 1996. Requisite role of angiopoietin-1, a ligand for the TIE2 receptor, during embryonic angiogenesis. Cell 87, 1171–1180.

Terman, B.I., Dougher-Vermazen, M., Carrion, M.E., Dimitrov, D., Armellino, D.C., Gospodarowicz, D., Bohler, P., 1992. Identification of the KDR tyrosine kinase as a receptor for vascular endothelial cell growth factor. Biochem. Biophys. Res. Commun. 187, 1579–1586.

Topper, J.N., Gimbrone Jr., M.A., 1999. Blood flow and vascular gene expression: fluid shear stress as a modulator of endothelial phenotype. Mol. Med. Today 5, 40–46.

Tskhovrebova, L., Trinick, J., 2002. Role of titin in vertebrate striated muscle. Philos. Trans. R Soc. Lond., B Biol. Sci. 357, 199–206.

van der Ven, P.F., Bartsch, J.W., Gautel, M., Jockusch, H., Furst, D.O., 2000. A functional knock-out of titin results in defective myofibril assembly. J. Cell Sci. 113 (Pt. 8), 1405–1414.

Xu, X., Meiler, S.E., Zhong, T.P., Mohideen, M., Crossley, D.A., Burggren, W.W., Fishman, M.C., 2002. Cardiomyopathy in zebrafish due to mutation in an alternatively spliced exon of titin. Nat. Genet. 30, 205–209.

Yang, X., Castilla, L.H., Xu, X., Li, C., Gotay, J., Weinstein, M., Liu, P.P., Deng, C.X., 1999. Angiogenesis defects and mesenchymal apoptosis in mice lacking SMAD5. Development 126, 1571–1580.

Ylikorkala, A., Rossi, D.J., Korsisaari, N., Luukko, K., Alitalo, K., Henkemeyer, M., Makela, T.P., 2001. Vascular abnormalities and deregulation of VEGF in Lkb1-deficient mice. Science 293, 1323–1326.